

An Engineering Approach to Improve Performance Predictions for Wind Turbine Applications: Comparison with Full Navier-Stokes Model and Experimental Measurements

M. N. Hamlaoui^{1,2}, A. Bouhelal^{1†}, A. Smaili¹ and H. Fellouah³

¹ *Laboratory of Green and Mechanical Development (LGMD), National Polytechnic School -ENP-, P.B. 182 El-Harrach, Algiers, 16200, Algeria*

² *Department of Civil Engineering, University of Ferhat Abbas-Setif 1, Route de Bejaia, Setif, Algeria*

³ *Department of Mechanical Engineering, University of Sherbrooke, 2500 Boulevard de l'Université, Sherbrooke (QC) J1K2R1, Canada*

†Corresponding Author Email: abdelhamid.bouhelal@g.enp.edu.dz

ABSTRACT

Accurate predictions of aerodynamic performance and near wake expansion around Horizontal Axis Wind Turbine (HAWT) rotors is pivotal for studying wind turbine wake interactions and optimizing wind farm layouts. This study introduces a novel engineering model centered on stall delay correction to enhance the precision of the Actuator Disk Method (ADM) predictions in both aerodynamic performance and near wake expansion around HAWT rotors. The model is developed based on a comprehensive study of the 3D lift coefficient evolution over the rotor blade, incorporating a shift parameter that considers both stall angle detection and radial decrement. The proposed approach demonstrates remarkable agreements, showcasing discrepancies as low as 7% for both loads and axial wake predictions. These quantifiable results underscore the effectiveness of the model in capturing intricate aerodynamic phenomena. Looking forward, the success of this approach opens avenues for broader applications, guiding future research in wind energy towards improved simulation accuracy and optimized wind farm designs.

Article History

Received October 26, 2023

Revised February 10, 2024

Accepted February 18, 2024

Available online April 30, 2024

Keywords:

Aerodynamics

Wind energy

Effect of rotation

Near wake

Full Navier-Stokes

Actuator disk

1. INTRODUCTION

Over the last decade, the importance of environmental sustainability has grown dramatically, not only in satisfying the world's energy demand, but also in decreasing negative environmental consequences. With the Paris agreement (Rhodes, 2016) setting the bar high, energy producers are striving to develop technologies that not only meet the energy demand, but also contribute to a cleaner and safer environment.

According to the International Renewable Energy Agency (IRENA) report for 2019 (IRENA, 2019), wind energy technology has seen significant development, and the projected electricity generation based on renewables is expected to reach 86% by 2050, with wind power accounting for one-third of this percentage. However, designing effective Horizontal Axis Wind Turbines (HAWT) is crucial to reduce energy costs, as an uncertain knowledge of the loads leads to over-designed systems and higher energy costs (Rehman et al., 2018).

To predict the aerodynamic performances of wind turbines, various numerical methods are available. The Blade Element Momentum (BEM) method is a fundamental technique used to calculate the aerodynamic performance of wind turbines (Hamlaoui et al. 2018; Bouhelal et al. 2023a). However, this method is limited in its ability to simulate the flow field and wind farms. In contrast, Computational Fluid Dynamics (CFD) methods are the most precise and commonly used approaches to study both performance and wake aerodynamics of wind turbines (Snel, 2003; Bouhelal et al., 2018a; Ramesh Kumar & Selvaraj, 2023). Mainly, two approaches, to fulfill the CFD simulations, are available based on the rotor representation: (i) the hybrid methods where the rotor is modeled as a mathematical body force within an actuator disc (ADM) (Conway, 1998; Masson et al., 2001; Hamlaoui et al., 2021a), an actuator line (ALM) (Sørensen & Myken, 1992) in addition of the actuator surface (Dobrev et al., 2007) and (ii) the real geometry approach (also designated: the Full Navier-Stokes approach) (Bouhelal et al., 2017; Bouhelal et al. 2018a; Bouhelal et al. 2018b; Bouhelal et al. 2023b), in which the real complex geometry of the blades is implemented into the

NOMENCLATURE			
ADM	Actuator Disk Method	LES	Large Eddy Simulation
ALM	Actuator Line Method	PIV	Particle Image Velocimetry
B	rotor number of blades	RANS	Reynolds Averaged Navier-Stokes
c	local chord at given radial station	r	local radial station
CFD	Computational Fluid Dynamics	R	rotor radius
C_l	corrected lift coefficient	TSR, (or λ)	Tip Speed Ratio
C_d	corrected drag coefficient	U_0	free stream velocity
Cl_{inv}	inviscid lift coefficient	U_n	normal component of the flow velocity relative to blade local station
C_n	normal force coefficient	U_{rel}	flow velocity relative to blade local station
C_t	tangential force coefficient	U_t	tangential component of the flow velocity relative to blade local station
f_l	separation factor for the lift coefficient variation	α	angle of attack
f_d	separation factor for the drag coefficient variation	α_s	stall angle of attack
f_n	axial volume force component	β	twist angle
FNS	Full Navier-Stokes model	γ	coning angle
f_t	tangential volume force component	θ_0	pitch angle
f_s	shift parameter	φ	flow angle
HAWT	Horizontal Axis Wind Turbines	Ω	rotational speed

computational mesh. From a technical standpoint, the simplified approaches are most used, for wind farms analyses, because of their less expensive calculation time and hardware requirements.

Choi et al. (2013) used a full Navier-Stokes approach, including the nacelle and tower of 2 MW wind turbines, to conduct a wind farm simulation and determine the best arrangement. They found an optimal separation distance of 5D, where D is the rotor diameter. AbdelSalam and Ramalingam (2014) conducted wake analyses of the 3bladed 180 kW Danwin HAWT using both full Navier-Stokes and actuator disk approaches. They simulated turbulence using the standard $k-\epsilon$ turbulence model and found that the full Navier-Stokes simulation showed better agreement with the measured data than the actuator disk predictions, which tended to underestimate the wake deficit. To model the effect of wind turbine wake interactions on HAWT performance, Sturge et al. (2015) proposed a new hybrid actuator disk and full Navier-Stokes approach. Mainly, they validated the far wake velocity field obtained using the actuator disk approach with wind tunnel measurements and then implemented it for Full Navier-Stokes computations. The collected data revealed a considerable loss in power production from the downstream turbine when subjected to the upstream turbine's wake.

Bouhelal et al. (2018a) studied the impacts of four distinct Reynolds Averaged Navier-Stokes (RANS) turbulence models on two near-wall approaches employing high and low Reynolds models for HAWT performance predictions using the full Navier-Stokes computational technique. They found that all the investigated models provided good predictions for low incoming wind speeds, while for high incoming wind speeds, the high Reynolds version of the RNG $k-\epsilon$ model was considered to be the best performance predictor.

Stevens et al. (2018) conducted wind farm simulations using Large Eddy Simulations (LES) and compared ADM and ALM forecasts to wind tunnel results. They discovered that the ADM predictions gave good wake and performance estimation with fewer mesh and computational cost requirements than the ALM. Based on the ADM predictions, Tian et al. (2020) conducted a comparative study of the impact of various turbulence models on the wake behavior downstream from the HAWT rotor and discovered that the wake stream predictions were particularly sensitive to the implemented turbulence model, with a maximum difference of 40%.

The hybrid methods (simplified geometry methods) are known for providing reliable and consistent predictions of HAWT performance as well as good wake behavior under attached flow conditions. However, these methods can break down when stall occurs and separated flow conditions arise due to the effect of rotation. To account of this effect, several approaches have been proposed to correct the 2D wind tunnel measured airfoil aerodynamic characteristics, such as the stall delay models developed by Snel et al. (1994), Du and Selig (1998), Chaviaropoulos and Hansen (2000), Lindenburg (2004), and Dumitrescu and Cardos (2009), which are among the most well-known.

Breton et al. (2008) investigated six well-known stall delay models and assessed their dependability using the NREL Phase VI HAWT model. Their findings revealed that the rotational augmentation phenomena is complicated and difficult to forecast, particularly at high wind speeds. Amini et al. (2021) presented changes to the empirical coefficients of Snel et al.'s (1994) stall delay model and studied their impact on the MEXICO rotor using ADM in OpenFOAM. Despite substantial improvements, major disparities in load forecasts were seen with no validation using other HAWT types.

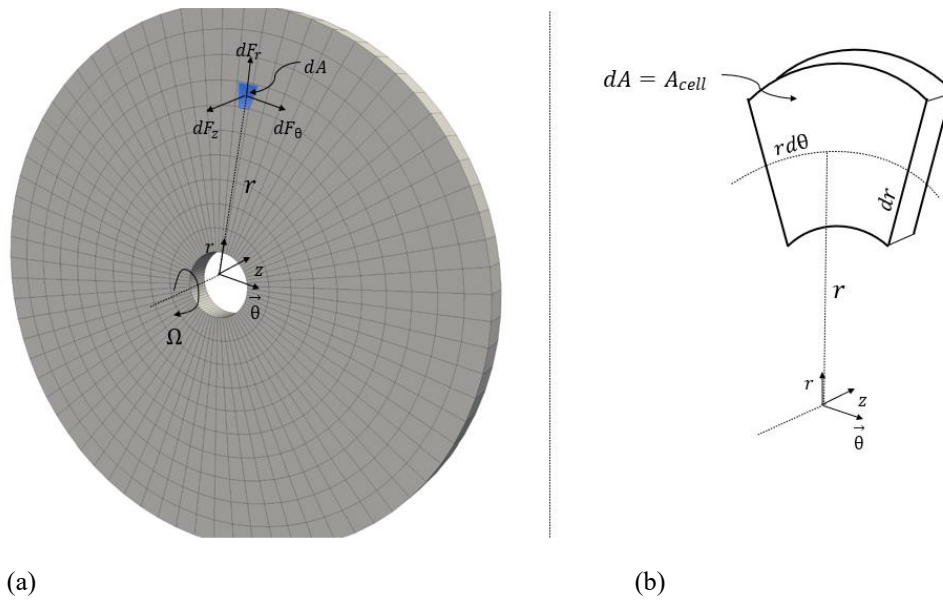


Fig. 1 Actuator disk concept illustrating (a) mesh configuration and (b) elementary forces distributions

Recently, Hamlaoui et al. (2021b) proposed a stall delay model for the lift and drag coefficients correction. The lift coefficient correction model has been carried out based on fitting the 3D aerodynamic characteristics extracted through an inverse ADM where the drag coefficient correction model has been extracted by recalibrating stall delay model proposed by Chaviaropoulos and Hansen (2000). The proposed model was validated throughout two commonly used experimental wind turbine models, namely MEXICO and NREL Phase VI, see Ref. (Hamlaoui et al., 2021b). Their findings offer a promising alternative for accurately predicting wind turbine performance under rotating conditions.

This study aims to investigate the aerodynamic performance and rotor near wake predictions of a HAWT at stall conditions using both the actuator disk method and full Navier-Stokes approaches. An engineering stall delay model has been introduced and implemented to account of the effect of rotation. The study validates its findings using New MEXICO PIV measurements and compares its results with the well-known stall delay model of Snel et al. (1994). For the aerodynamic performance study, primarily the expected torque, the normal and tangential sectional forces distribution over the rotor blade at two incoming wind speeds of 15 m/s and 24 m/s, corresponding respectively to the design and fully detached flow conditions, have been investigated using both numerical approaches and compared with measured data. Then, a quantitative study of the near wake on the vicinity of the MEXICO rotor has been carried out and validated versus the New MEXICO PIV measurements (Schepers et al., 2014; Boorsma & Schepers, 2016). As the effect of rotation consists on radial flow appearance and loads increase (axial induction augmentation), mainly, the axial distributions at distances of $\pm 3R$ for radial stations of $0.5R$ and $1.5R$, the radial distributions at a distances of $\pm 0.13R$ upstream and downstream from the rotor of the axial and radial velocity components have been carried out and validated at stall conditions. This study provides new insights into the HAWT performance and near wake

predictions at stall conditions, which can improve the design and efficiency of modern wind turbines.

2. MATHEMATICAL MODEL

2.1 Actuator Disk Model

The actuator disk concept consists of mathematical modeling of the real geometry of HAWT rotor where a predefined cylindrical actuator disk volume, defined by the rotor swept area (A), describes the real rotor effect on the flow field. The external forces exerted by the HAWT rotor are computed at each mesh cell located inside the predefined cylindrical actuator disk volume as depicted in Fig. 1(a), these loads act against the incoming flow yielding static pressure jump. For a typical HAWT rotor blades with a coning angle of $\gamma = 0$, the actuator disk geometry is a cylinder with a radius of R . As the actuator disk concept assumes that the HAWT rotor blade aerodynamic loads do not have any radial force component ($dF_r = 0$), the elementary actuator disk surface generated forces are decomposed mainly into axial dF_z and tangential dF_θ force components.

The Blade Element theory has been usually applied for the aerodynamic estimation of loads along HAWT rotor blades. A standard HAWT rotor typically comprises B blades, each with a radius of R , a rotational speed denoted by Ω , and an overall pitch angle represented by θ_0 . For modern and efficient HAWT, the rotor blade chord c and geometric twist β vary radially, from the root to the tip of the rotor blade, in order to maintain the rotor optimal performances. For a given blade span point r , as depicted in Fig. 2, the relative velocity (U_{rel}) can be primarily broken down into its predominant normal and tangential components (U_n, U_t):

$$U_{rel} = \sqrt{U_n^2 + U_t^2} \quad (1)$$

$$\text{where } U_n = -u_j z_j \text{ and } U_t = (\Omega r - u_j \theta_j) \quad (2)$$

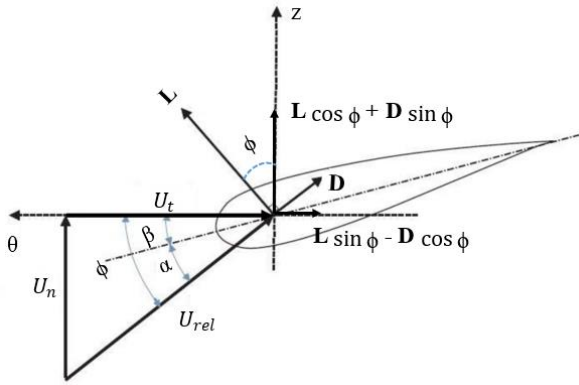


Fig. 2 Sectional forces and velocity vectors relative to the blade radial station

u_j represents the velocity component, z_j and θ_j are considered as the cosine direction of both the unit vectors z and θ .

The definition of the angle of attack (α) is articulated as follows:

$$\alpha = \arctan \left(\frac{U_n/U_t}{-(\beta + \theta_0)} \right) \quad (3)$$

In order to account of the infinite number of blades assumption, the tip loss correction approach of [Shen et al. \(2005\)](#) has been applied and is expressed as follows:

$$F = \frac{2}{\pi} \cos^{-1} \left[\exp \left(-g \frac{B(1 - (r/R))}{2(r/R) - \sin \phi} \right) \right] \quad (4)$$

$$g = \exp[-a(B\lambda - b)] + 0.1 \quad (5)$$

where a and b are constants of 0.125 and 21 respectively.

Based on the blade element theory, the yielding blade sectional forces in the axial f_z and tangential f_θ direction at a given radial station r is expressed as follows:

$$f_z = (1/2)F\rho U_{rel}^2 c(C_l \cos \phi + C_d \sin \phi) \quad (6)$$

$$f_\theta = (1/2)F\rho U_{rel}^2 c(C_l \sin \phi - C_d \cos \phi) \quad (7)$$

The resulting external forces exerted by the rotor computed at discrete point defining the mesh cell center located inside the predefined cylindrical actuator disk volume (see Fig. 1(b)) are expressed as follows:

$$dF_{cell,i} = B f_i dr \frac{rd\theta}{2\pi r} = \frac{B}{2\pi} f_i \frac{A_{cell}}{r} \quad (8)$$

The source term S_i defining the external forces exerted by the rotor is introduced in the momentum equation as a volume force which yields the following expression:

$$S_i = A_{cell} i / V_{cell} \quad (9)$$

2.2 Existing Stall Delay Models (ESDM)

In order to account of the mostly encountered 3D rotational effect, several approaches have been presented in the literature where most of them share the same correction methodology for airfoil aerodynamic characteristics (C_l , C_d) which are expressed as follows:

$$C_l = C_{l,2D} + f_l \Delta C_l \quad (10)$$

$$C_d = C_{d,2D} + f_d \Delta C_d \quad (11)$$

where: f_l and f_d represent, respectively, the airfoil aerodynamic characteristics separation factors.

$\Delta C_l = C_{l,inv} - C_{l,2D}$ is the difference between the potential lift coefficient and the 2D measured lift coefficient.

$C_{l,inv} = 2\pi(\alpha - \alpha_0)$ and α_0 represents the angle of attack obtained at the zero-lift coefficient.

$\Delta C_d = C_{d,2D} - C_{d,0}$ is the discrepancy between the 2D drag coefficient, obtained from wind tunnel measurements, and the drag coefficient at an α of zero.

In this study, the most well-known stall delay model of [Snel et al. \(1994\)](#) has been applied and is expressed as follows:

$$f_l = a_s (c/r)^n \quad (12)$$

$$f_d = 0 \quad (13)$$

where a_s and n are empirical constants which varies, respectively, between 2 to 3 and 1 to 2. In the present study, the values of 3 and 2, proposed by [Amini et al. \(2021\)](#), have been chosen for the empirical coefficient a_s and n respectively (i.e., $f_l = 3(c/r)^2$).

2.3. ESDM limitations

Despite the fact that current HAWT are variable speed and/or variable pitch regulated, stalling remains unavoidable in the lower mid-span area of the rotor blade due to the Coriolis and centrifugal forces impact. Figure 3(a) shows that the recorded 3D experimental lift coefficient at the blade radial station of $r/R = 0.3$ possess a specific evolution versus the angle of attack. It can be noticed that it rises with the increase of the angle of attack to achieve the utmost value at an angle of attack (3D stall angle α_s) much higher than the 2D one; once this angle is exceeded, the empirical lift coefficient decrement is recorded which reveals the stall occurrence. The ESDM are based on their modeling philosophy, on sectional corrections of the stationary airfoil aerodynamic properties by estimating a certain constant, considered as the rate of augmentation due to the effect of rotation. This correction methodology, for all the incoming wind speeds, yields linear evolution of the corrected lift coefficient which can be explained physically, as it has been detailed in Ref. ([Hamlaoui et al., 2021a](#)), that stall, using ESDM, has been delayed to infinity causing significant over prediction of loads. The present limitation constitutes an ultimate paradox with the definition of the effect of rotation ([Snel et al., 1994](#); [Du & Selig, 1998](#); [Dumitrescu & Cardos, 2009](#); [Narramore & Vermeland, 1992](#)) which is the delay of the 2D stall α to a higher one (α_s) providing the HAWT performances increase.

In addition of the first limitation, most of the ESDM formulations presented in the literature are based on the

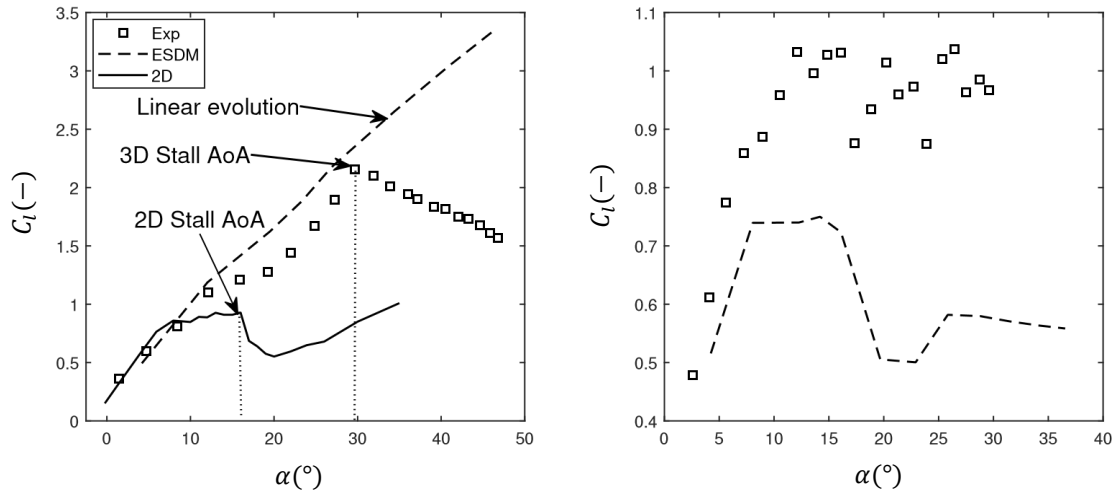


Fig. 3 The 3D lift coefficient estimated over the NREL Phase VI rotor blade at span wise positions of a) $r/R = 30\%$ and b) $r/R = 80\%$ obtained using existing stall delay models (Hamlaoui et al., 2021b)

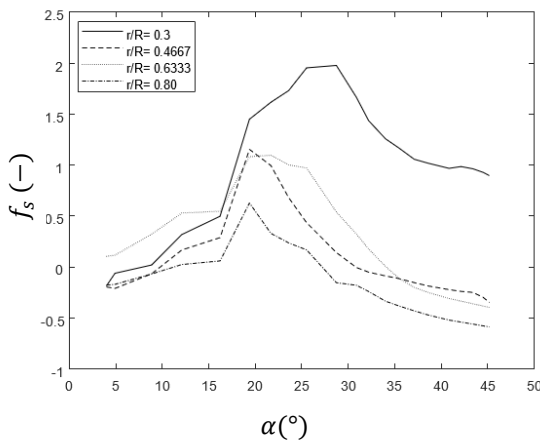


Fig. 4 Experimental evolutions of f_s versus the angle of attack for different radial stations over the NREL Phase VI rotor blade using the inverse-ADM (Hamlaoui et al., 2021b)

aspect ratio (c/r) in order to ensure the radial decrements. As HAWT are a high aspect ratio rotating machines, it has been explained also in Ref. (Hamlaoui et al., 2021a) that the fact of using this decrement methodology causes significant under predictions of lift coefficient at near the tip region of the rotor blade as shown in Fig. 3.(b). These nonrealistic modeling and limitations confirm the conclusions of Breton et al. (2008) that none of the proposed correction approaches, available in the literature, are able to describe in a suitable manner the rotational augmentation effect due to the lack of generality.

2.4 Solution based on New Stall Delay Approach (NSDA)

As the NREL Phase VI is the only HAWT in the literature on which the 3D experimental airfoil characteristics are available for all the incoming wind speeds, in Ref. (Hamlaoui et al., 2021a) a deep study on the 3D lift coefficient evolution over the rotor blade, have been carried out, at four radial stations of $r/R = 30\%$, $r/R = 46.67\%$, $r/R = 63.33\%$ and $r/R = 80\%$, neglecting the

span wise station of $r/R = 0.95$ mainly affected by the blade tip loss, in the purpose of taking into account the ESDM limitations. Based on the experimental behaviors of the shift parameter f_s , defined in Eq (14), which represents the amount of increase (percentage) variation versus the angle of attack obtained at four span wise stations over the NREL Phase VI rotor blade (Fig. 4); they illustrated that the extent of augmentation at each radial position over the rotor blade varies versus the recorded α and the attained radial stations simultaneously. So, they concluded that for a more realistic modeling of the effect of rotation. The proposed correction approach should consider both the stall angle of attack (α_s) detection and the radial decrement.

$$f_s = \frac{C_{l\ exp} - C_{l\ 2D}}{C_{l\ 2D}} \quad (14)$$

Based on these two main considerations, they proposed an original correlation for the lift coefficient correction, based on the shift parameter, composed of two functions ensuring both the radial decrements and the 3D stall angle detection expressed as follows:

$$f_s \left(\alpha, \frac{r}{R} \right) = a \left(1 - \left(\frac{r}{R} \right)^2 \right) \exp \left[- \left(\frac{\alpha - \alpha_s}{d} \right)^2 \right] \quad (15)$$

The alteration concerning α is achieved through the utilization of a Gaussian function, wherein parameters a , α_s , and d denote the amplitude, the angle of attack corresponding to the peak (the 3D stall angle), and the controlling peak width, respectively. A mean value has been suggested for each parameter, as shown in Table 1.

Unlike the lift coefficient, it has been found in Ref. (Hamlaoui et al., 2021a) that the drag coefficient evolution could be assumed as linear. Thus, they proposed recalibration of the mostly well-known Chaviaropoulos and Hansen (2000) drag coefficient correction model, providing on its original form significant over-predictions (Breton et al., 2008; Guntur & Sørensen, 2013), to improve its predictions and expressed as follows:

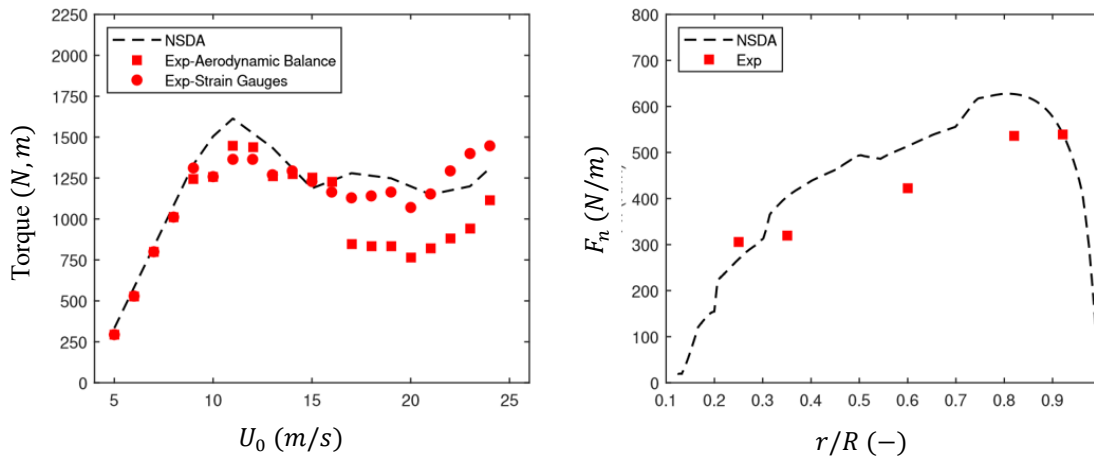


Fig. 5 (a) Mechanical torque predictions for the NREL Phase VI rotor and (b) The normal force radial distribution over the MEXICO rotor blade obtained for an incoming free stream velocity of 24 m/s, obtained using the NSDA model

Table 1 NSDA and Proposed model suggested coefficients

Coefficients	<i>a</i>	α_s	<i>d</i>
NSDA	1.8	25	9.5
Proposed model	1.55	$24,96(r/R)^{-0,117}$	9.5

$$f_d = a_h \left(\frac{c}{R}\right)^h \cos^n \beta \tag{16}$$

where a_h has been set to a value of 1.2 instead of 2.2, $h=1$ and $n=4$.

The application of the new proposed correction approach to the NREL Phase VI wind turbine has shown noticeable improvement and high accuracy where a very low discrepancies have been recorded for the predicted rotor torque as shown in Fig. 5(a). Nevertheless, high over estimations of the normal force distribution over the MEXICO rotor has been recorded as shown in Fig. 5(b). More details on the NSDA validations are presented in Ref. (Hamlaoui et al., 2021a).

As it has been explained previously, the effect of rotation encountered on HAWT rotating blades is mainly characterized by two main specifications mentioned as follows:

- The impact of rotation is noteworthy at the radial stations near the root of the rotor blade and decreases radially by getting further from it to attain the 2D effect at the near tip region of the rotor blade.
- The impact of rotation delays the 2D separation of the angle of attack to a higher one (α_s) at each span wise position depending on the significance of the 3D effect.

Based on the foregoing features, it is possible to conclude that as the influence of rotation significance varies radially, so does the 3D stall angle along the spanwise direction of the rotor blade.

For a more realistic modeling and more improvement of the NSDA predictions; in this paper, a simple correlation describing the radial variation along the rotor

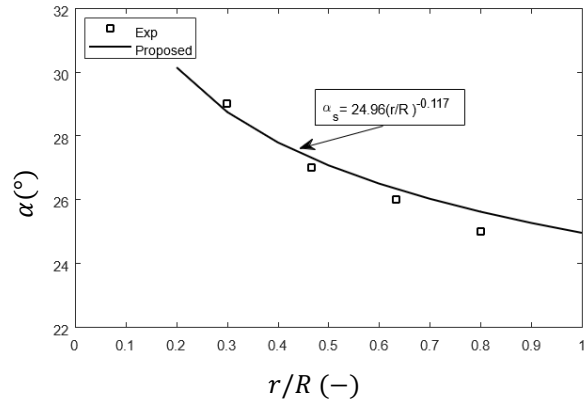


Fig. 6 Proposed correlation for the stall angle radial variation.

blade of the 3D stall angle (α_s) has been proposed based on the empirical 3D stall angles variation over the NREL Phase VI as shown in Fig. 6.

In addition, the stall angle α_s radial variation affects the obtained peak values at each radial station which require the recalibration of the proposed amplitude. As a result, a new value of the amplitude *a* has been proposed in this paper where both the new proposed stall angle expression and the amplitude value are given in Table 1.

3. MATHEMATICAL MODEL

In the present study, the Reynolds Averages Navier Stokes (RANS) formulation has been used in order to describe the flow field in vicinity of HAWT rotor yielding the time averaged equations depicted as follows:

$$\frac{\partial u_r}{\partial x_i} = 0 \tag{17}$$

$$u_j \frac{\partial u_r}{\partial x_j} = -\frac{1}{\rho} \frac{\partial p}{\partial x_i} + \frac{\partial}{\partial x_j} \left[(\nu + \nu_t) \frac{\partial u_r}{\partial x_j} \right] + \delta S_i \tag{18}$$

where $\delta = 0$ for the Full Navier-Stokes approach (FNS), and $\delta = 1$ for the Actuator Disk Model (ADM).

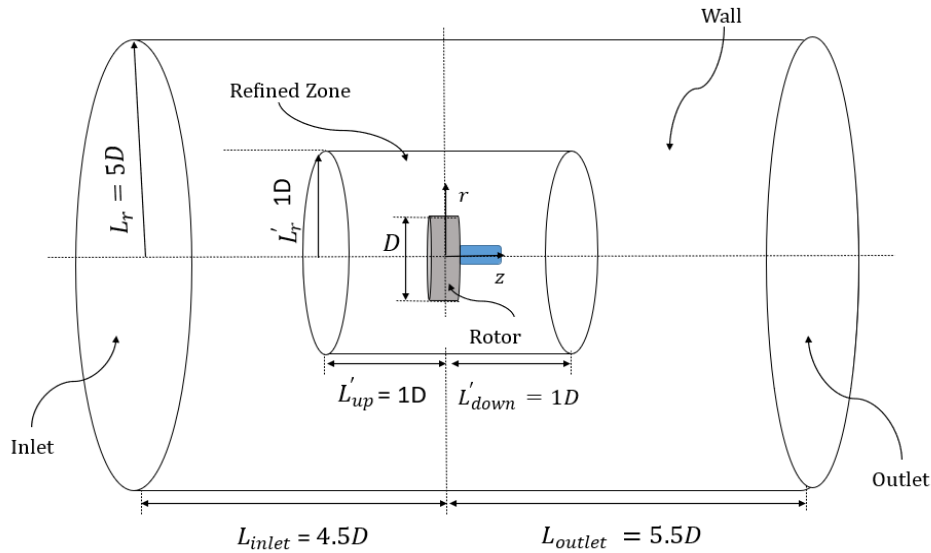


Fig. 7 Computational domain for the ADM configuration

In the Eqs. (17) and (18), u_r is the relative velocity including the Coriolis and the centripetal accelerations for the FNS, and it equals the mean fluid velocity u_i for the ADM, p represents the pressure, ν and ν_t are mainly the kinematic laminar and turbulent viscosity respectively and S_i is the added source term representing the actuator disk effect on the flow field.

For the enclosing the RANS equations (Eqs. (17) and (18)), the RNG $k-\varepsilon$ two equations turbulence model of Yakhot and Orszag (1986) has been applied. Since it has proven its high efficiency in prediction in comparison to its low price in previous studies (Bouhelal et al., 2018a).

4. NUMERICAL METHOD

The numerical simulations, for both the ADM and the Full Navier-Stokes equations (FNS) approaches were carried out using Navier-Stokes finite volume discretization schemes based on cylindrical coordinates. The SIMPLE (Semi Implicit Method for Pressure-Linked Equation) (Patankar, 2018) algorithm has been used for the equations system solving where relaxation factors of 0.3 and 0.7 have been set for the pressure and other variables respectively (Bouhelal et al., 2018a).

Concerning the interpolation schemes, the second order difference scheme has been applied for the spatial term of the Navier-Stokes equation discretization where a second order Gauss Upwind scheme has been used for the convective term.

The boundary layers setup has been described as follows:

- **Inlet:** homogeneous velocity, turbulence kinetic energy and its dissipation rate fields have been carried out in addition of a zero gradient for the pressure field has been set. For the ADM configuration, the turbulent parameters k_0 and ε_0 have been estimated rooted on OpenFOAM user guide (Greenshields et al. 2015).

- **Outlet:** where a pressure outflow condition has been specified for the pressure, a zero-axial gradient for the velocity, turbulence kinetic energy, and dissipation rate fields has been given.

- **Walls:** using the logarithmic velocity scale wall functions given in Eq. (19) to prescribe a no slip requirement for the nacelle, a slip condition has been established for the lateral wall boundary condition:

$$u^+ = \frac{1}{\kappa} \log_{10} E y^+ \quad \text{for } y^+ \geq 11.225 \quad (19)$$

Noting that the nacelle geometry has been ignored in the FNS configuration, as suggested by Bouhelal et al. (2018a). The choice of the computational domain and the mesh sensitivity study of the two numerical approaches would be discussed separately.

4.1 Actuator Disk Model (ADM)

As reported earlier by Hamlaoui et al. (2022), the yielding optimized computational domain, described in Fig. 7, applied for the ADM calculation consists of cylinder with a radius and a length along the axial direction at the edge of $L_r = 5D$ and $10D$ respectively divided rooted on the position of the rotor center. The inlet and outlet boundary conditions have been located at distances of $L_{inlet} = 4.5D$ and $L_{outlet} = 5.5D$ upstream and downstream from the rotor center respectively. A refined zone, in the axial direction, of $L'_{up} = L'_{down} = 1D$ upstream and downstream from the rotor center respectively with a radius of $L'_r = 1D$ has been defined to account of high fluid properties recorded gradients.

A mesh sensitivity analysis was conducted utilizing the MEXICO wind turbine characteristics. The study focused on an incoming wind speed of $U_0 = 15$ m/s (i.e., design wind speed) to determine the most effective mesh discretization for computations using the ADM in the proximity of the HAWT rotor. Ensuring precise predictions in the near wake of the HAWT rotor necessitates a thorough examination of mesh dependency in both upstream and downstream directions from the

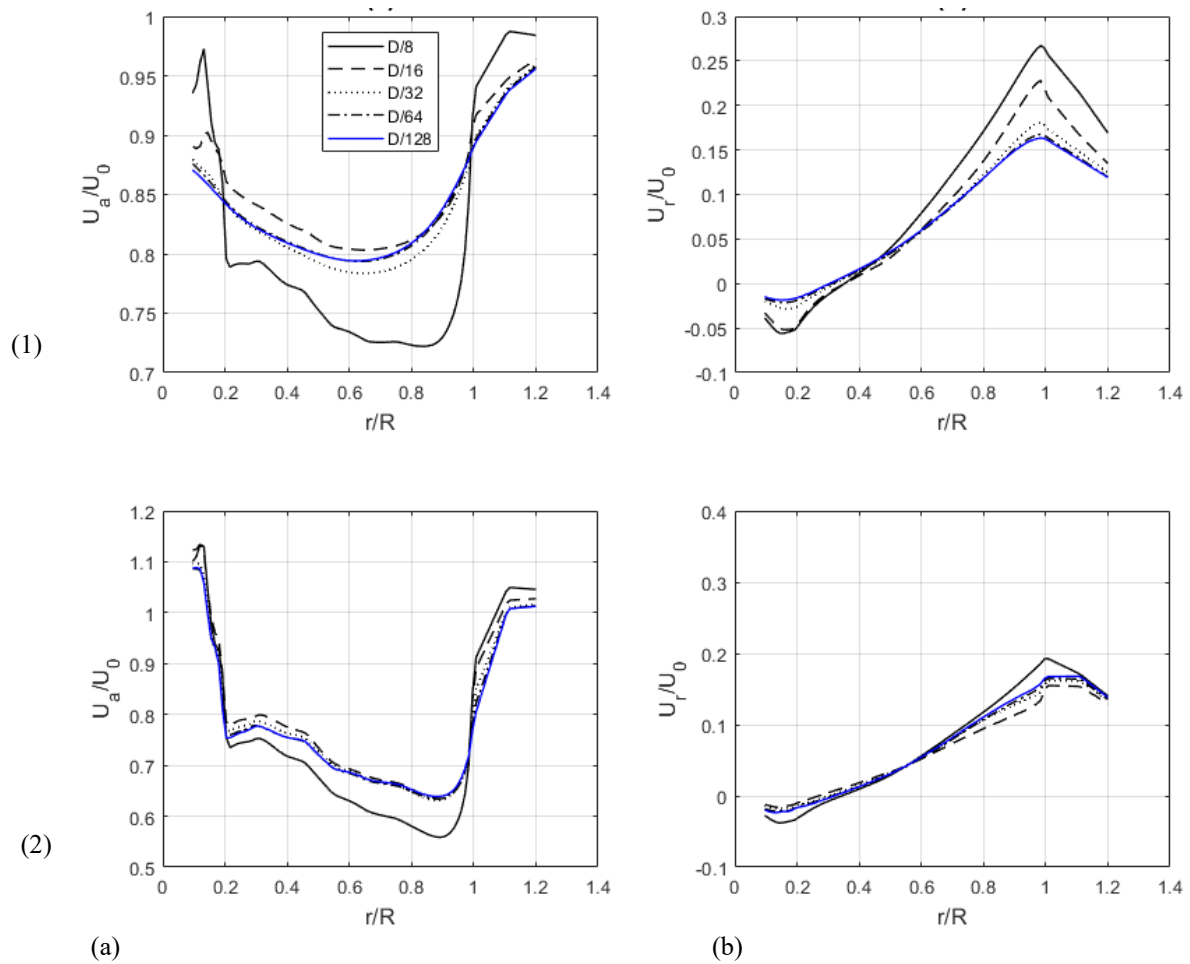


Fig. 8 ADM mesh sensitivity study based on the radial distribution of the (a) axial and (b) radial velocity components for (1) upstream and (2) downstream from the rotor obtained at a distance of $z/R = \pm 0.13$ from the rotor center.

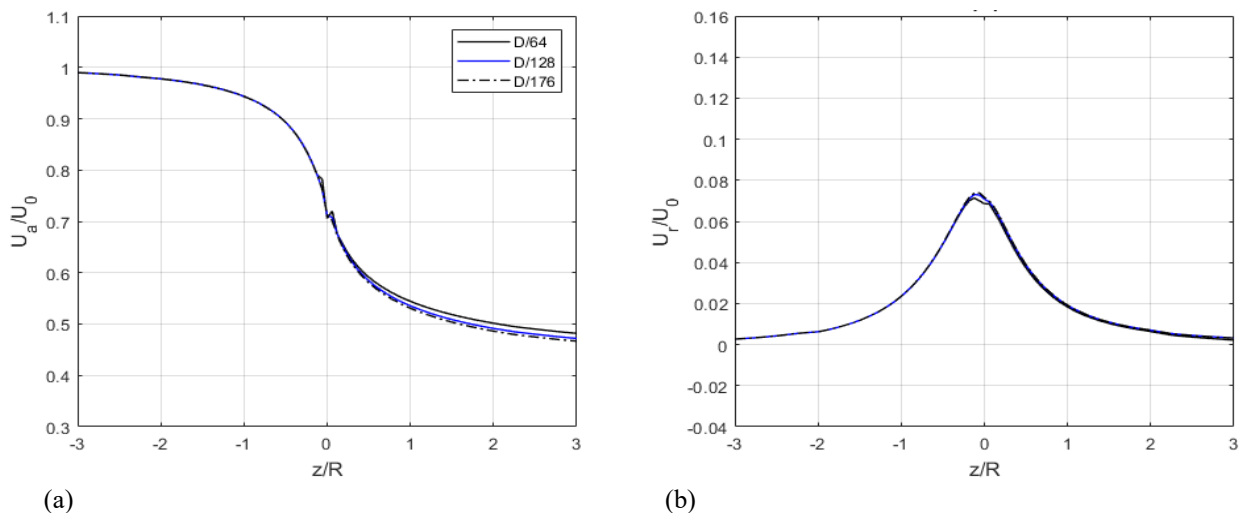


Fig. 9 ADM mesh sensitivity study based on the axial distribution of the (a) axial and (b) radial velocity components upstream and downstream from the rotor obtained at an axial distance of $z/R = \pm 0.13$.

rotor center. Five mesh sizes have been proposed, representing $D/8$, $D/16$, $D/32$, $D/64$, and $D/128$, respectively. The findings, presented in Fig. 8, indicate minimal variations in axial and radial velocity components at a distance of $z/R = -+0.13R$ upstream and downstream from the rotor when employing a mesh resolution of $D/64$. However, an analysis of the axial distribution of velocity components, illustrated in Fig. 9,

reveals oscillations at the rotor plane, indicating the need for further mesh refinement to enhance predictions. Subsequent refinement of the mesh demonstrated that a resolution of $D/128$ is optimal for adequately capturing the flow field in the vicinity of the HAWT rotor. The actual ADM mesh, using this optimal resolution of $D/128$, comprises a total of 4 million cells.

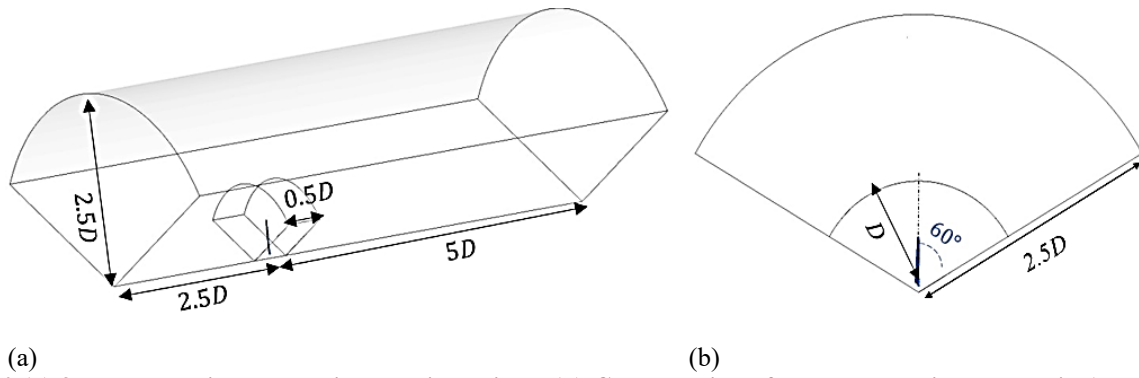


Fig. 10 (a) 3D computational domain and dimensions, (b) Cross-section of the computational domain (Bouhelal et al., 2018a)

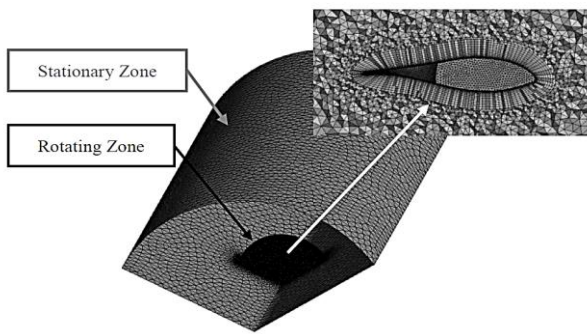


Fig. 11 Computational domain generated for Full Navier-Stokes case

4.2 Full Navier-Stokes (FNS)

As it has been described by Bouhelal et al. (2018a), the full Navier-Stokes approach simulations have been carried out for full rotor geometry including the blades. In order to reduce computational time and mesh requirements, the flow field in the vicinity of the MEXICO rotor has been considered as symmetrical; thus, the computational domain has been carried out for only one blade representing one-third of the full rotor geometry and exploiting the 120° symmetry of the computational domain.

The yielding computational domain, shown in Fig. 10 (a), consists of third of a cylinder with a radius of $2.5D$ and an edge length of $7.5D$ in the axial direction decomposed based on the rotor center position. The inlet boundary of the computational domain has been located at a distance of $2.5D$ upstream from the rotor center where the outlet has been located at a distance of $5D$ downstream from the rotor center. The computational domain is mainly constituted of rotating and stationary regions; the small zone close to the rotor blade, as shown in Fig 10(b), constitutes the rotating part of the domain with a diameter of D and an axial thickness of $D/2$ allowing both the rotor blades rotation and the mesh refinement near the rotor blades geometry.

The optimized mesh required for the one-third computational domain, using high Reynolds turbulence model, contains approximately 4.1×10^6 of nodes. The rotating domain has been discretized with about 3.4×10^6 million of nodes, as shown in Fig. 11, on which 107380

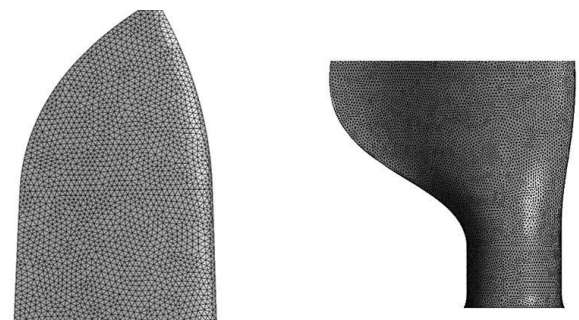


Fig. 12 Details of the mesh on the blade surface at (left) tip region and (right) root region

nodes have been prescribed at the blade surface (see Fig. 12). The height of the first-floor mesh element close to the blade is of approximately 4×10^{-5} m ensuring that the y^+ parameter is between 30-200 at the blade surface (logarithmic wall function region). A boundary layer mesh of 20 parallel lines near the blade surfaces has been created using the prismatic layers technique. For more details about the computational domain and mesh sensitivity test, see Bouhelal et al. (2018a) and Bouhelal et al. (2022b).

5. NEW MEXICO MEASUREMENTS

In the present study, simulations have been carried out on the MEXICO rotor since the New MEXICO experiments (Schepers et al., 2014; Boorsma & Schepers, 2016) represent the only full-scale measurements providing both the aerodynamic performances and the flow characteristics in the vicinity of HAWT rotor. The New MEXICO measurements (Schepers et al., 2014; Boorsma & Schepers, 2016) have been carried out in the Large-Scale Low Speed Facility (LLF) of the German Dutch Wind Tunnels (DNW) in 2014 where the data has been provided through the MexNext project's collaboration.

5.1 The MEXICO rotor

The MEXICO wind turbine is a three blades 4.5 m diameter upwind HAWT with a speed of rotation of 425 rpm in the Clockwise direction. Its geometric properties (chord and twist) vary radially from the root to the tip of the rotor blade, as shown in Fig. 13, to ensure an optimum operation condition. The MEXICO rotor blade consists of

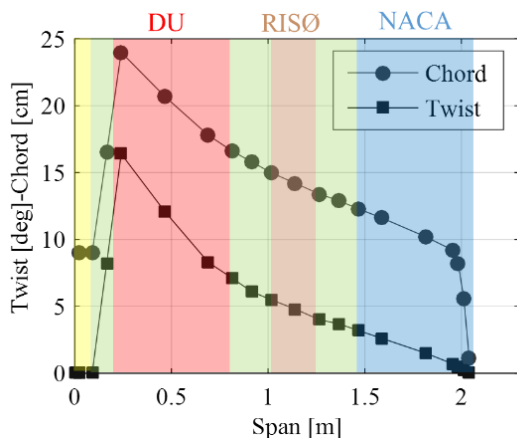


Fig. 13 MEXICO wind turbine chord and twist variation along the span direction

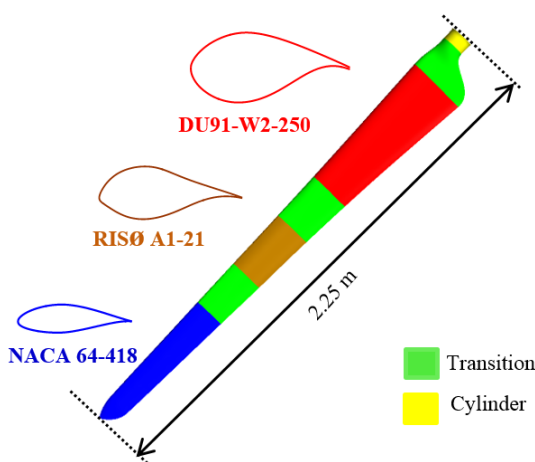


Fig. 14 MEXICO blade and its airfoils configurations (Bouhelal et al (2018a))

a global pitch angle and a coning angle of -2.3° and $\gamma = 0^\circ$ respectively. It is constituted of a huge nacelle of 2.5 m in length and 0.54 m diameter (Bouhelal et al., 2023b); the nacelle nose cone has been simplified as the composition of frustum and half sphere of 0.4 m in length and 0.3 m diameter respectively.

The MEXICO rotor blade, as illustrated in Fig. 14, is composed of three different aerodynamic profiles DU91-W2-250, RISØA1-21 and NACA64-418 linked by aerodynamic transitions which are situated as follows:

1. The DU91-W2-250 profile is applied from 20% to 45.5% span wise position.
2. The RISØ-A1-21 profile is applied from 54.4% to 65.5% radial station.
3. The NACA 64-418 profile is applied from 74.4% to the tip of the rotor blade.

5.2 Experimental Setup

The experimental measurements of the New MEXICO have been carried for three main wind speeds of $U_0 = 10$ m/s (TSR= 10), $U_0 = 15$ m/s (TSR= 6.67) and $U_0 = 24$ m/s (TSR= 4) corresponding to low speed, designed speed and detached flow speed respectively Schepers et

al. (2014). The wind turbine model has been instrumented with unsteady pressure sensors at five radial stations of $r/R = 25\%$, $r/R = 35\%$, $r/R = 60\%$, $r/R = 82\%$ and $r/R = 92\%$, respectively, distributed over the three blades. Phase locked stereo PIV measurements have been carried at the 9 o'clock plane of the rotor, as shown in Fig. 16, for several configurations and locations in order to characterize the near wake flow features in the vicinity of the HAWT rotor and to verify the stream tube theory assumptions. Velocity profiles were measured in different axial and radial transverse positions as shown in Fig. 16. The axial lines cover 10 m from upstream to downstream, whereas the radial lines cover about 3 m in the near wake (see Fig.15).

6. RESULTS

The current simulations aim to explore the performance of Horizontal Axis Wind Turbines (HAWT) and predict near wake characteristics under design and stall conditions. This involves employing both the actuator disk (ADM) and full Navier-Stokes (FNS) approaches. Consequently, the investigation is divided into two focal areas: aerodynamic performance and near wake predictions around the MEXICO rotor.

6.1 Aerodynamic Study

For the aerodynamic performance study, mainly the predicted torque, the normal and tangential sectional forces distribution over the rotor blade at two incoming wind speeds of 15 m/s (TSR= 6.67) and 24 m/s (TSR= 4.17) have been investigated using both the numerical approaches and compared with measured data. The normal and tangential forces in both the FNS and experimental data were determined exclusively through the integration of pressure, with the omission of consideration for shear stresses.

o Blade Forces

Radial distribution of the measured and computed normal and tangential forces, at five span wise positions of $r/R = 0.25$, $r/R = 0.35$, $r/R = 0.60$, $r/R = 0.82$ and $r/R = 0.92$, over the MEXICO rotor blade has been carried out for two incoming wind speeds of $U_0 = 15$ m/s and $U_0 = 24$ m/s corresponding to design and separated flow regimes as illustrated in Fig. 17 and Fig. 18.

The design speed case (TSR= 6.67), as shown in Fig. 19.(a), has been characterized as the onset of stall where deviation has been detected at the outer part of the blade near the root of the rotor at radial stations $r/R < 0.25$. It can be noticed that the radial flow begins to appear at the separated region; however, the flow is dominant in the chord wise direction, thus, the influence of centrifugal forces could be neglected. It can be seen, in Fig. 17, that the predictions of the ADM including both stall delay correction models, are almost similar for both the tangential and normal forces distribution except the model of Snel et al. (1994) which provides certain over estimation of the tangential force component for radial stations below $r/R < 0.25$ at the separated flow region. The predictions show in general good agreements between the experimental data and ADM calculations.

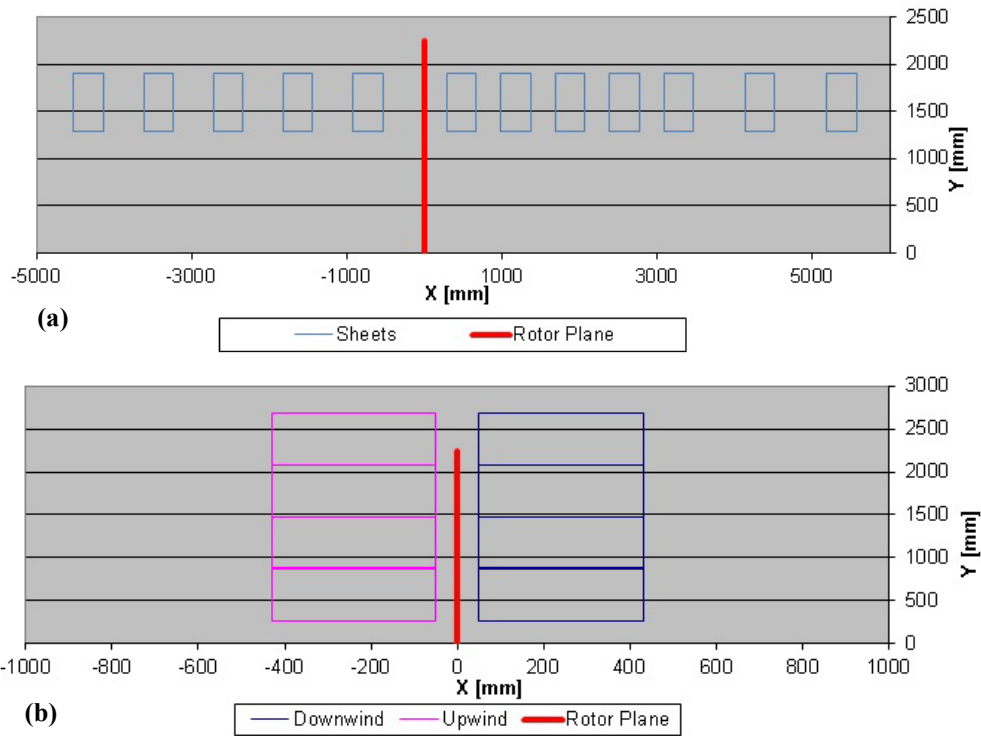


Fig. 15 (a) Axial and (b) Radial sheets traverses of the New Mexico PIV measurements (Schepers et al., 2014)

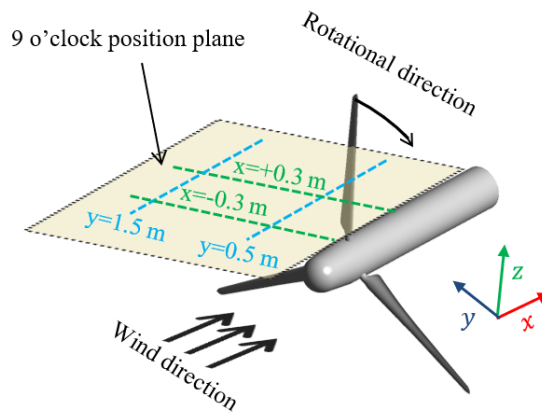


Fig. 16 Overview of the PIV measurements on the MEXICO wind turbine (Bouhelal et al (2023))

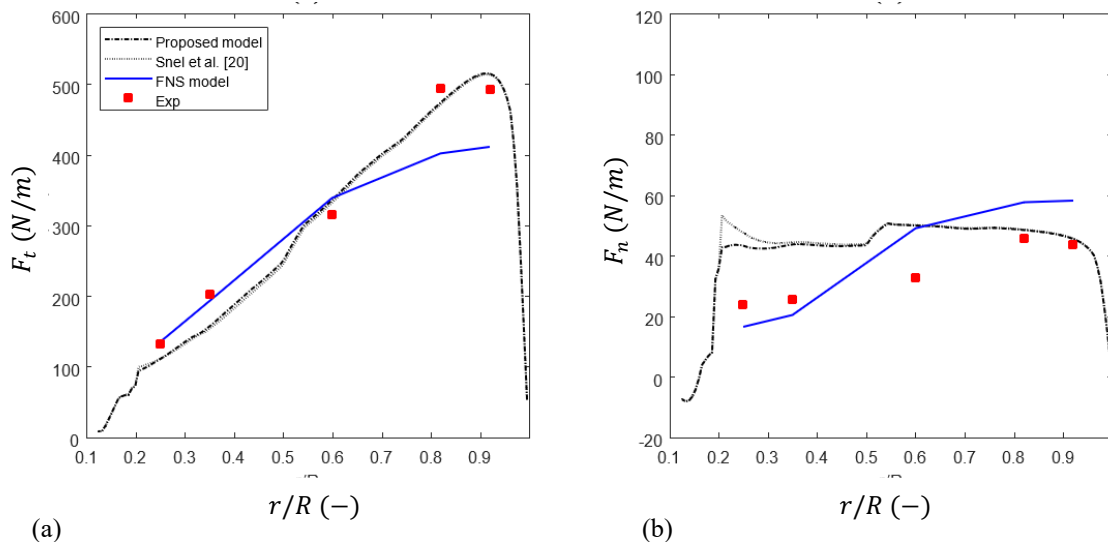


Fig. 17 Radial distribution of the (a) normal and (b) tangential forces over the rotor blade at TSR of 6.67

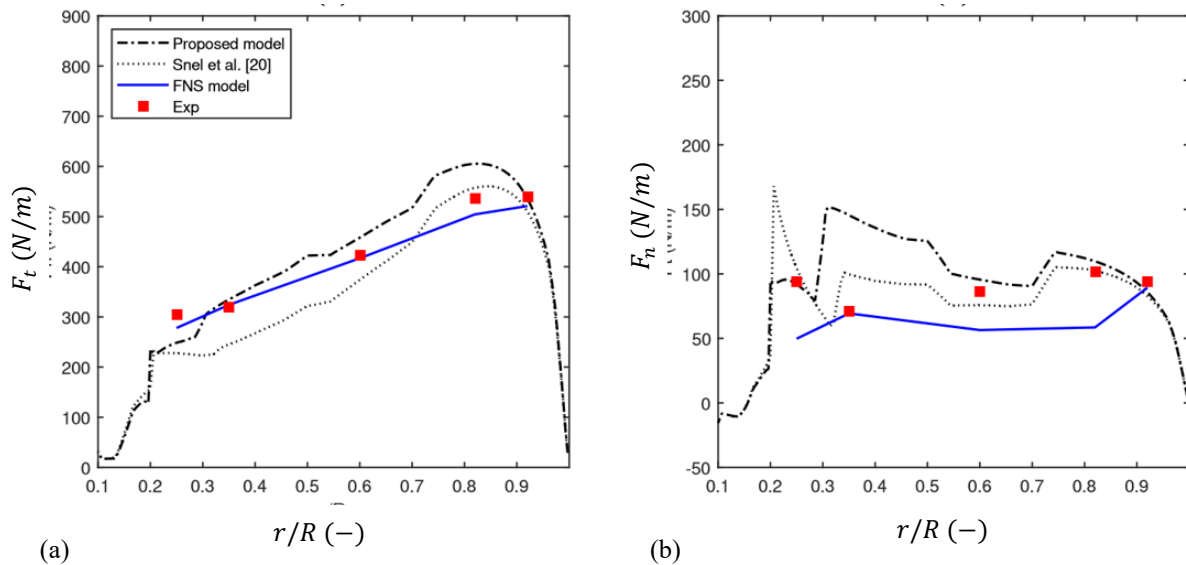


Fig. 18 Radial distribution of the (a) normal and (b) tangential forces over the rotor blade at a TSR of 4.17

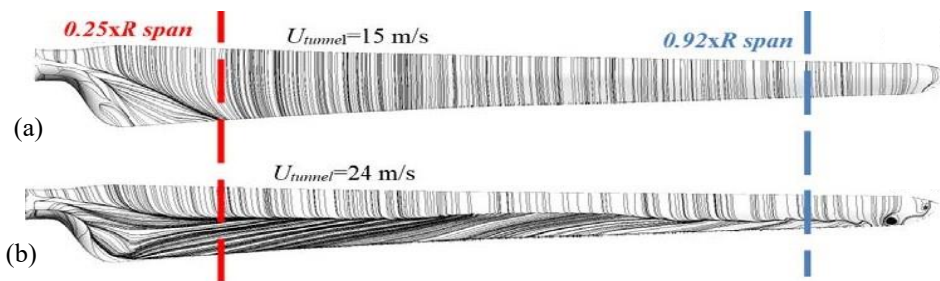


Fig. 19 Velocity streamlines on the suction side of the MEXICO rotor blade for design TSR= 6.67 and separated TSR= 4.17 flow regimes (calculated using FNS approach).

The FNS model computations has provided also good agreement with both the measured normal and tangential forces distribution especially at the lower mid-span region of the rotor blade; nevertheless, by getting closer to the tip of the blade, the FNS model computations tends to underestimate the normal force component which could be due to the high loss on the rotor blade, at this region, which results in lower calculations of pressures at the blade than real measurements. For the tangential force component, it can be seen that some discrepancies between both the numerical calculation approaches and measurements are recorded and must be pointed out. It should be noted that computations are very sensitive in the tangential direction where pressure gradients are confronted in the leading and trailing edges which causes major differences in measurements. The separated flow case (TSR= 4.17), as shown in Fig. 19.(b), has been characterized as massive flow detachment accompanied with radial flux creation causing the fluid particles to congregate in the center of the rotor blade airfoil (chord wise direction) forming a mass of fluid that travels radially due to the significance of centrifugal forces.

It can be seen, in Fig. 18, that the predictions, using Snel et al. (1994), of the normal and tangential force components are significantly under-predicted compared to measurements where high discrepancies are recorded compared to experimental data. Using the NSDA model as shown in Fig. 5.(b), the over estimations recorded at the upper mid-span region of the rotor blade could be due to

averaged 3D stall angle (α_s) assumption that leads to an overprediction of the estimated 3D lift coefficient values by getting nearer from the tip region of the rotor blade. By taking into account the 3D stall angle radial variation, it can be seen that the introduction of the proposed model has shown significant improvement of the predictions where good agreement with the experimental measurements over the rotor blade has been recorded providing the most accurate estimations compared to the existing models. The FNS model predictions have provided high accuracy with the measured normal force distribution over the rotor blade; however, significant underestimations have been recorded for the tangential force component which could affect the resulting aerodynamic torque prediction.

○ **Torque Prediction**

Figure 20 shows the predicted mechanical torque through the MEXICO rotor. It can be noticed that the obtained performances can be divided into two parts of study: attached flow regime for incoming wind speeds $U_0 < 15$ m/s (TSR > 6.67) and detached flow regime for incoming wind speeds $U_0 > 15$ m/s (TSR < 6.67). It can be seen that for an attached flow regime corresponding to incoming wind speeds lower than 15 m/s (TSR > 6.67), the predicted torque using both Snel et al. (1994) and the proposed model give good agreements compared to the rotor torque measurements except the FNS model computations where certain under-prediction of about 20% has been recorded. The present under-estimation

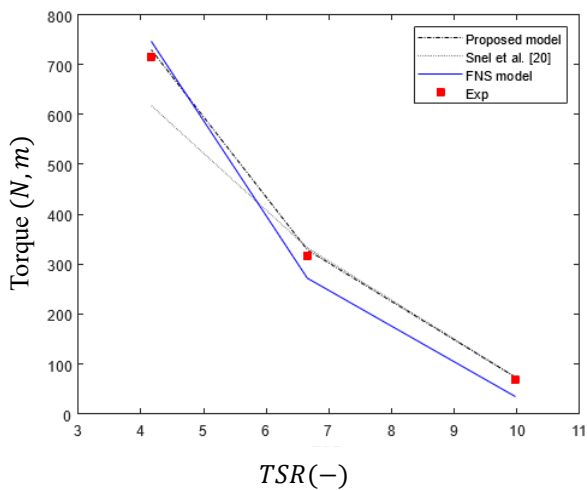


Fig. 20 Predicted torque of the MEXICO rotor

Table 2 Comparison between computed and measured torque for the three studied wind speeds

Wind speeds	10 m/s	15 m/s	24 m/s
Measurements (Schepers et al., 2014)	68	316	715
FNS (Bouhelal et al., 2018a)	33	270	744
Snel Model (Snel et al., 1994)	70	328	616
Proposed ADM	69.4	327.5	727
Relative error (%) of the proposed ADM	2.06	3.64	1.68

could be related to the limitations of the utilized high Reynolds number $k-\epsilon$ RNG turbulence model to solve boundary layer accurately for low incoming wind speeds. However, for high incoming wind speeds $U_0 > 15$ m/s ($TSR < 6.67$), where stall is deeply present and have a significant effect, the FNS model simulations have provided good agreements with the measured data with a relative error of 4.2%. For the ADM computations, remarkable under-predictions, using the stall delay model of Snel et al. (1994), of about 21% have been observed compared to the experimental measurements. The application of the proposed model has provided noticeable improvement and high accuracy agreements to the measured rotor torque with a low discrepancy of about 1.8% especially for high wind speeds (or low TSR values).

Table 2 presents the computed average values of torque for both studied models, proposed ADM and FNS, in comparison to experimental measurements and Snel’s model. As seen in this table, the maximum relative error for the proposed ADM does not exceed 3.7%, demonstrating the effectiveness of the proposed engineering approach.

6.2 Near Wake Velocity Study

Most of the engineering models, found in the literature, for stall delay correction are based on HAWT aerodynamic performances (power, torque, blade loads, etc.) reproduction in order to ensure the validity of their approaches. However, the flow field in vicinity of the rotor

(near wake) is affected directly by the presence of the rotor blades. As a results, good predictions of the loads over the rotor blade should reproduce the same flow field in the upstream and down stream directions.

The purpose of the present study is to assess the capability of the proposed numerical approach for the flow field reproduction around the rotor where the effect of the predicted loads is significant and directly affect the resulting velocity field. Quantitative comparison of the ADM and FNS model computations has been carried out with phase locked stereo PIV measurements at the 9 o’clock plane of the rotor for several configurations and location corresponding to:

- the axial velocity distribution of the axial and radial velocity components at radial station of $r= 1.5$ m, 9 o’clock positioned, for incoming wind speeds of 15 m/s (design case) and 24 m/s (fully separated case) flow regimes as shown in Fig. 21.
- the radial velocity distribution of the axial and radial velocity components at axial stations of $z= - 0.3$ m and $z= 0.3$ m upstream and downstream from the rotor respectively, 9 o’clock positioned, for incoming wind speeds of 15 m/s (design case) and 24 m/s (fully separated case) flow regimes as shown in Fig. 22 and Fig. 23.

Figure 21 shows the axial velocity distribution of the axial and radial velocity components at radial station of $r= 1.5$ m, 9 o’clock positioned, for incoming wind speeds of 15 m/s (design case) and 24 m/s (fully separated case) flow regimes. For incoming wind speed of 15 m/s, it can be seen that the FNS model computations and the ADM calculations using both the stall delay models are slightly underestimating the velocity deficit/creation of the axial/radial velocity component compared to experimental measurements; however, the overall trend is very well maintained. In contrary to the design case, for incoming wind speed of 24 m/s, the effect of rotation appears causing remarkable underprediction of both the velocity deficit of the axial velocity component and the radial flow appearance for the ADM calculation using the stall delay model of Snel et al. (1994) due to the under-estimation of the normal force component over the rotor blade (as shown in Fig. 17.(a)) causing an alleviation of the rotor axial induction.

Nevertheless, as the FNS and the proposed models have provided good predictions of the normal force component over the rotor blade, it can be seen that the velocity deficit of the axial velocity component and the radial flow creation in the span wise direction have been estimated accurately where the proposed model predictions provide the best fitting compared to measured data. It should be noted that a better estimation of the axial velocity induction is primordial and represents key parameter especially when studying the interaction of wind turbines situated in wind farms. Figure 22 and Fig. 23 show the radial velocity distribution of the axial and radial velocity components at axial stations of $z= -0.3$ m and $z= +0.3$ m upstream and downstream from the rotor respectively, 9 o’clock positioned, for incoming wind

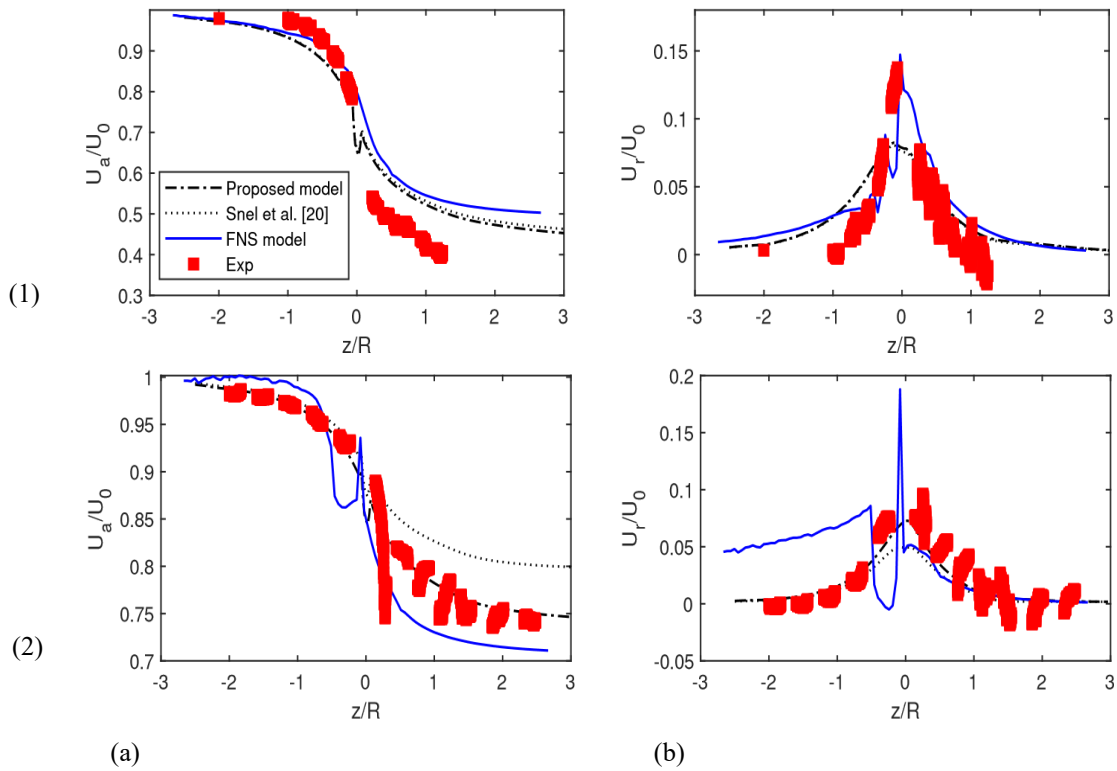


Fig. 21 Axial velocity distribution of the (a) axial and (b) radial velocity components at radial station of $r=1.5$ m, 9 o'clock positioned, for incoming wind speeds of (1) 15 m/s (design case) and (2) 24 m/s (fully separated case) flow regimes

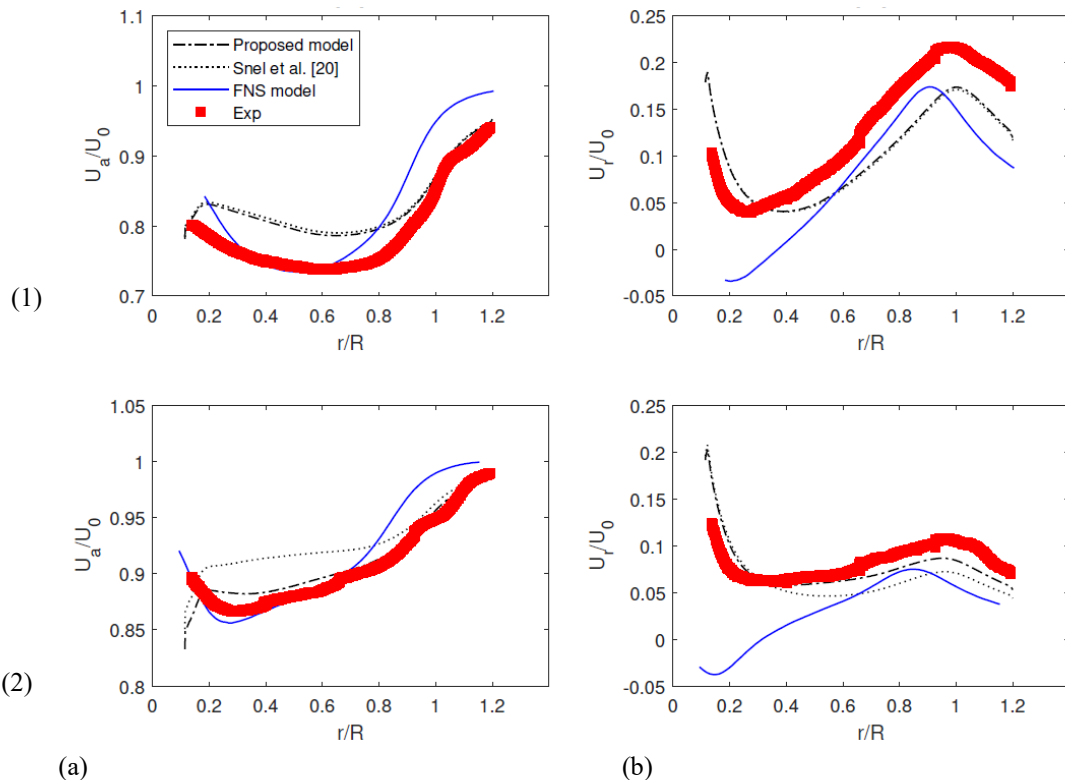


Fig. 22 Radial velocity distribution of the (a) axial and (b) radial velocity components at an axial station of $z=-0.3$ m downstream from the rotor, 9 o'clock positioned, for incoming wind speeds of (1) 15 m/s (design case) and (2) 24 m/s (fully separated case) flow regimes

speeds of 15 m/s (design case) and 24 m/s (fully separated case) flow regimes. For the design flow case, it can be noticed that the ADM calculations using Snel stall delay model and the proposed model, for both the cases

upstream and downstream from the rotor, tends to underestimate the velocity deficit of the axial velocity component as well as the radial flow creation compared to the measured data. Even if the overall allure is well

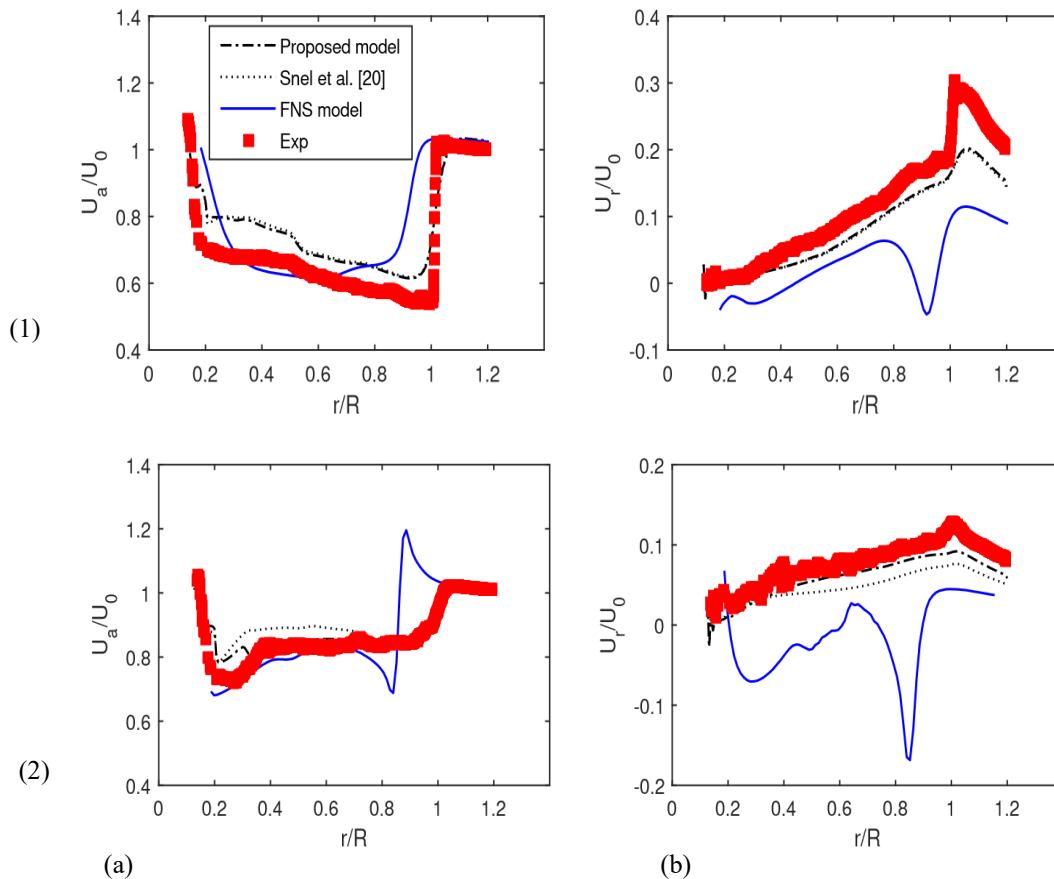


Fig. 23 Radial velocity distribution of the (a) axial and (b) radial velocity components at an axial station of $z = +0.3$ m downstream from the rotor, 9 o'clock positioned, for incoming wind speeds of (1) 15 m/s (design case) and (2) 24 m/s (fully separated case) flow regimes

maintained, discrepancies are still recorded. In contrary to the ADM predictions, it can be seen that the FNS model computations provide the best fitting compared to measured data for both the axial and radial velocity components. For the fully separated case, where the centrifugal forces are effective, it can be noticed that significant under-estimations of both the axial velocity component deficit and the radial velocity creation, based on the ADM calculations using Snel stall delay model, have been recorded because of their non-realistic modeling of the effect of rotation. Even though the FNS model computations have shown good agreements with the normal force component over the rotor blade at stall conditions, it can be seen that it fails to predict in a suitable manner the radial velocity component at the axial stations of $z = -0.3$ m and $z = +0.3$ m upstream and downstream from the rotor. In contrary to Snel stall delay model and the FNS model predictions, the Proposed model have provided noticeable improvement where good predictions of both the axial velocity component and the radial flow appearance, over the rotor blade span direction, have been recorded compared to the experimental measurements.

Based on the present quantitative near wake study, it could be concluded that the proposed engineering model for the stall delay correction provides more realistic modeling of the effect of rotation resulting on high accuracy predictions in the vicinity of the HAWT rotor.

7. DISCUSSION OF RESULTS

The presented results provide a comprehensive exploration of HAWT performance, focusing on aerodynamic characteristics and near wake predictions under design and stall conditions. The study utilizes both actuator disk and full Navier-Stokes approaches, offering a detailed analysis of the MEXICO rotor.

7.1 Broader Impacts of the Findings

- **Stall Characteristics:** The study identifies the onset of stall conditions, particularly at the design speed case (TSR=6.67). Understanding that stall behaviors and deviations in blade characteristics is crucial for optimizing wind turbine performance and reliability.
- **Model Validation:** The comparison between numerical predictions and experimental data for both aerodynamic forces and torque demonstrates the effectiveness and limitations of different modeling approaches. This validation is critical for the wind energy community, providing confidence in the accuracy of simulation tools.
- **Unique Experimental Insights:** The deep study on the 3D lift coefficient evolution over the rotor blade, particularly focusing on the NREL Phase VI

turbine, offers unique experimental insights. The availability of comprehensive 3D experimental airfoil characteristics for all incoming wind speeds distinguishes this work in the literature.

- **Enhanced Correction Models:** The proposed correction approach, considering both the stall angle of attack (α_s) detection and the radial decrement, showcases an innovative method to enhance lift and drag coefficient predictions. This is crucial for more accurate modeling of the effect of rotation, especially near the root of the rotor blade.
- **Influence of Flow Separation:** The investigation of separated flow regimes (TSR=4.17) highlights the impact of massive flow detachment and radial flux creation on blade performance. This insight is valuable for designing turbines that can operate efficiently under varying wind conditions.
- **Comprehensive Flow Field Assessment:** The near wake velocity study expands the investigation beyond aerodynamic forces and torque, providing a comprehensive assessment of the flow field around the rotor. This holistic approach is crucial for understanding the impact of predicted loads on the resulting velocity field.
- **Importance of Axial Velocity Induction:** The study emphasizes the significance of accurately estimating axial velocity induction, a key parameter for studying wind turbine interactions in wind farms. The findings contribute to the broader understanding of wind turbine wake dynamics.

7.2 Uniqueness of the Current Work

- **Improved Stall Delay Modeling:** The introduction of a new stall model that considers the radial variation of the 3D stall angle (α_s) is highlighted as a novel contribution. This model demonstrates significant improvements in predicting normal and tangential force components over the rotor blade, especially in separated flow conditions.
- **Torque Prediction Enhancement:** The study proposes a model that significantly improves torque predictions, especially in detached flow regimes. This enhancement is crucial for accurate assessment and optimization of wind turbine performance, particularly at high wind speeds.
- **Shift Parameter (f_s):** The introduction of the shift parameter (f_s) based on the experimental behaviors of the NREL Phase VI rotor blade is a significant departure from previous correction models. The shift parameter considers both radial decrements and 3D stall angle detection, leading to a more realistic modeling approach.
- **Calibration of Drag Coefficient Correction Model:** The recalibration of the [Chaviaropoulos and Hansen \(2000\)](#) drag coefficient correction model, considering linearity in the drag coefficient evolution, demonstrates a novel approach to

improving predictions. These addresses previous issues of over-predictions in the original model.

- **Flow Field Influence:** The near wake velocity study highlights the direct influence of rotor blades on the flow field in the upstream and downstream directions. This consideration sets the current work apart from previous studies that primarily focused on reproducing aerodynamic performances.
- **Realistic Rotation Modeling:** The proposed engineering model for stall delay correction is uniquely tailored to provide a more realistic representation of the effect of rotation, resulting in high-accuracy predictions in the vicinity of the HAWT rotor. This novel approach distinguishes the current study from existing literature, such as [Snel et al. \(1994\)](#), [Breton et al. \(2008\)](#) and [Guntur and Sørensen \(2013\)](#).

7.3 Novel Findings

- **Model-Specific Discrepancies:** The study identifies discrepancies between numerical models and experimental data, emphasizing the sensitivity of computations in tangential directions and the impact on torque predictions. Such insights are valuable for refining numerical models and improving their accuracy.
- **Flow Regime-Dependent Accuracy:** The study distinguishes between attached and detached flow regimes, showcasing different accuracies in torque predictions based on incoming wind speeds. This understanding aids in developing models that can adapt to various operational conditions.
- **Lift Coefficient Correction:** The proposed lift coefficient correction model, incorporating a Gaussian function for α variation, showcases noticeable improvement and high accuracy in predicting rotor torque. However, overestimations of the normal force distribution over the MEXICO rotor indicate potential areas for refinement.
- **Radial Variation of 3D Stall Angle (α_s):** The proposal of an original correlation describing the radial variation of the 3D stall angle along the rotor blade provides a key element for more realistic modeling. This recognizes the radial variation of the effect of rotation, a crucial consideration for accurate predictions.
- **Axial and Radial Velocity Components:** The study presents detailed quantitative comparisons of axial and radial velocity components at various radial and axial stations. Model-specific discrepancies are identified, such as underestimations in the velocity deficit and radial flow creation for certain models under specific conditions.
- **Impact of Rotation:** The findings underscore the impact of rotation on the accuracy of predictions, especially at higher wind speeds. The study reveals how rotation-related underestimations can affect

the axial induction and, consequently, the overall performance of the turbine.

7.4 Direction for Future Research

- **Turbulence Model Refinement:** Addressing the limitations of the turbulence model for high incoming wind speeds should be a focus for future research. Developing or refining turbulence models to accurately capture boundary layer effects is essential for improving overall simulation accuracy.
- **Advanced Torque Prediction Models:** Building on the proposed model, future research could explore advanced methods for predicting torque under a broader range of conditions, including turbulence effects and dynamic stall situations.
- **Refinement of Lift Coefficient Correction:** Further research could focus on refining the lift coefficient correction model, especially in addressing the observed overestimations of the normal force distribution. This could involve additional empirical studies or adjustments to the proposed correlation.
- **Experimental Validation:** Continuation of experimental validation efforts will be crucial for refining and enhancing numerical models. Collaborative efforts between experimentalists and modelers can contribute to more accurate and reliable wind turbine simulations.
- **Interactions in Wind Farms:** Given the importance of axial velocity induction for studying wind turbine interactions in wind farms, future research could delve into more complex scenarios involving multiple turbines. This could provide insights into optimizing wind farm layouts for enhanced overall efficiency.

8. CONCLUSION

This study has presented a simple engineering model that effectively captures the stall delay phenomenon, enhancing predictions of aerodynamic performance and flow field characteristics near Horizontal Axis Wind Turbine (HAWT) rotors. Utilizing Reynolds Averaged Navier-Stokes equations coupled with the RNG $k-\epsilon$ turbulence model, the proposed model was integrated into the Actuator Disk Method (ADM) subroutine and rigorously validated against both Full Navier-Stokes (FNS) simulations and detailed Particle Image Velocimetry (PIV) measurements, particularly under stall conditions.

Quantitative assessments revealed excellent agreement between the proposed stall delay model and the FNS model, as well as experimental data, with a maximum error of merely 7%. This level of accuracy signifies the robustness of the proposed model in capturing the intricate dynamics associated with stall delay. The simplicity of the proposed model adds to its appeal, presenting a viable tool for the comprehensive

study of wind turbine interactions and the optimization of wind farms.

The successful implementation of the engineering model not only advances the understanding of stall delay but also holds significant implications for practical applications. By improving the accuracy of predictions in both aerodynamic performance and flow field characteristics, the proposed model contributes to the refinement of wind turbine simulation tools. This, in turn, aids in the optimization of wind farm layouts and enhances the overall efficiency and reliability of wind energy systems.

Looking ahead, the success of the proposed engineering model in capturing stall delay phenomena and improving predictive capabilities offers exciting perspectives for future research and application. Further refinements and validations could extend the model's applicability to a broader range of wind turbine configurations and operational scenarios. The integration of real-time data assimilation techniques and machine learning algorithms may enhance the model's adaptability to dynamic wind conditions. Moreover, collaborative efforts between researchers, experimentalists, and industry stakeholders could facilitate the development of a standardized tool for assessing wind turbine interactions within complex wind farm layouts. The insights gained from this study pave the way for a more nuanced understanding of aerodynamic phenomena in wind energy, steering us toward more efficient, sustainable, and optimized wind power systems.

ACKNOWLEDGMENTS

The authors thank the Directorate-General for Scientific Research and Technological Development (DGSRTD) of Algerian government and the Natural Sciences and Engineering Research Council (NSERC) of Canada (RGPIN-2016-03995). The authors also thank Calcul Quebec and Compute Canada networks for HPC facilities used for simulations.

CONFLICT OF INTEREST

The authors declare no conflict of interest.

AUTHORS CONTRIBUTION

Mohammed Nadjib Hamlaoui: Methodology, Software, Validation, Formal Analysis, Investigation, Resources, Data Curation, Writing of the Original Draft; **Abdelhamid Bouhelal:** Methodology, Software, Validation, Formal Analysis, Investigation, Resources, Data Curation, Writing of the Final Manuscript, Review and Editing, Visualization, Text and Figure Formatting; **Arezki Smaili:** Review and Editing; **Hachimi Fellouah:** Review and Editing.

REFERENCES

AbdelSalam, A. M., & Ramalingam, V. (2014). Wake prediction of horizontal-axis wind turbine using full-

- rotor modeling. *Journal of Wind Engineering and Industrial Aerodynamics* 124, 7–19. <https://doi.org/10.1016/j.jweia.2013.11.005>
- Amini, S., Golzarian, M. R., Mahmoodi, E., Jeromin, A., & Abbaspour-Fard, M. H. (2021). Numerical simulation of the mexico wind turbine using the actuator disk model along with the 3d correction of aerodynamic coefficients in openfoam. *Renewable Energy*, 163, 2029–2036. <https://doi.org/10.1016/j.renene.2020.10.120>
- Boorsma, K., & Schepers, J. (2016). *Rotor experiments in controlled conditions continued: New mexico*. Journal of Physics: Conference Series, 753, 022004. <https://doi.org/10.1088/1742-6596/753/2/022004>
- Bouhelal, A., Ladjal, A., & Smaili, A. (2023a). *Blade element momentum theory coupled with machine learning to predict wind turbine aerodynamic performances*. AIAA SCITECH 2023 Forum. <https://doi.org/10.2514/6.2023-1153>
- Bouhelal, A., Smaili, A., Masson, C., & Guerri, O. (2017). Comparison of BEM and full Navier-Stokes CFD methods for prediction of aerodynamics performance of HAWT rotors. In *2017 International Renewable and Sustainable Energy Conference (IRSEC)* (pp. 1–6). IEEE. <https://doi.org/10.1109/icweaa.2018.8605050>
- Bouhelal, A., Smaili, A., Guerri, O., & Masson, C. (2018a). Numerical investigation of turbulent flow around a recent horizontal axis wind turbine using low and high Reynolds models. *Journal of Applied Fluid Mechanics* 11(1), 151–164. <https://doi.org/10.29252/JAFM.11.01.28074>
- Bouhelal, A., Smaili, A., Guerri, O., & Masson, C. (2023b). Numerical investigations on the fluid behavior in the near wake of an experimental wind turbine model in the presence of the nacelle. *Journal of Applied Fluid Mechanics* 16(1), 21–33. <https://doi.org/10.47176/jafm.16.01.1382>
- Bouhelal, A., Guerri, O., Smaili, A., & Masson, C. (2018b). *Contribution to the aerodynamic study of the air-sand flow around a wind turbine blade installed in desert environment of algeria*. 2018 International Conference on Wind Energy and Applications in Algeria (ICWEAA), IEEE. <https://doi.org/10.1109/ICWEAA.2018.8605050>
- Breton, S. P., Coton, F. N., & Moe, G. (2008). A study on rotational effects and different stall delay models using a prescribed wake vortex scheme and nrel phase vi experiment data. *Wind Energy*, 11(5), 459–482. <https://doi.org/10.1002/we.269>
- Chaviaropoulos, P. K., & Hansen, M. O. L. (2000). Investigating three-dimensional and rotational effects on wind turbine blades by means of a Quasi-3D navier-stokes solver. *Journal of Fluids Engineering*, 122(2), 330–336. <https://doi.org/10.1115/1.483261>
- Choi, N. J., Hyun Nam, S., Hyun Jeong, J., & Chun Kim, K. (2013). Numerical study on the horizontal axis turbines arrangement in a wind farm: Effect of separation distance on the turbine aerodynamic power output. *Journal of Wind Engineering and Industrial Aerodynamics*, 117, 11–17. <https://doi.org/10.1016/j.jweia.2013.04.005>
- Conway, J. T. (1998). Exact actuator disk solutions for non-uniform heavy loading and slipstream contraction. *Journal of Fluid Mechanics*, 365, 235–267. <https://doi.org/10.1017/s0022112098001372>
- Dobrev, I., Massouh, F., & Rapin, M. (2007). *Actuator surface hybrid model*. Journal of Physics: Conference Series, IOP Publishing. <https://doi.org/10.1088/1742-6596/75/1/012019>
- Du, Z., & Selig, M. (1998). *A 3-d stall-delay model for horizontal axis wind turbine performance prediction*. 1998 ASME Wind Energy Symposium. <https://doi.org/10.2514/6.1998-21>
- Dumitrescu, H., & Cardos, V. (2009). Inboard boundary layer state on wind turbine blades. *ZAMM-Journal of Applied Mathematics and Mechanics: Applied Mathematics and Mechanics*, 89(3), 163–173. <https://doi.org/10.1002/zamm.200800105>
- Greenshields, C. J., et al. (2015). *Openfoam user guide*. OpenFOAM Foundation Ltd, version, 3(1), 47. <https://doi.org/10.51560/ofj.v1.26>
- Guntur, S., & Sørensen, N. (2013). *A detailed study of the rotational augmentation and dynamic stall phenomena for wind turbines* [PhD thesis, Technical Univ. of Denmark], Lyngby, Denmark.
- Hamlaoui, M. N., Smaili, A., & Fellouah, H. (2018). *Improved bem method for hawt performance predictions*. 2018 International Conference on Wind Energy and Applications in Algeria (ICWEAA), IEEE. <https://doi.org/10.1109/icweaa.2018.8605096>
- Hamlaoui, M. N., Smaili, A., & Fellouah, H. (2021b). *New stall delay approach for hawt performance predictions using a cfd hybrid method*. AIAA Scitech Forum. <https://doi.org/10.2514/6.2021-0951>
- Hamlaoui, M., Smaili, A., & Fellouah, H. (2021a). Improved stall delay model for hawt performance predictions using 3d navier-stokes solver and actuator disk method. *Journal of Applied Fluid Mechanics* 15(1), 37–50. <https://doi.org/10.47176/jafm.15.01.32651>
- Hamlaoui, M., Smaili, A., Dobrev, I., Pereira, M., Fellouah, H., & Khelladi, S. (2022). Numerical and experimental investigations of hawt near wake predictions using particle image velocimetry and actuator disk method. *Energy*, 238, 121660. <https://doi.org/10.1016/j.energy.2021.121660>
- IRENA. (2019). *Future of wind: Deployment, investment, technology, grid integration and socio-economic aspects*. International Renewable Energy Agency,

- Abu Dhabi.
<https://doi.org/10.20508/ijrer.v9i3.9741.g7722>
- Lindenburg, C. (2004). *Modelling of rotational augmentation based on engineering considerations and measurements*. European Wind Energy Conference, London. pp. 22–25.
- Masson, C., Smaili, A., & Leclerc, C. (2001). Aerodynamic analysis of hawks operating in unsteady conditions. *Wind Energy*, 4(1), 1– 22. <https://doi.org/10.1002/we.43>
- Narramore, J., & Vermeland, R. (1992). Navierstokes calculations of inboard stall delay due to rotation. *Journal of Aircraft*, 29(1), 73–78. <https://doi.org/10.2514/3.46127>
- Patankar, S. (2018). *Numerical heat transfer and fluid flow*. Taylor & Francis. <https://doi.org/10.1201/9781482234213>
- Ramesh Kumar, K., & Selvaraj, M. (2023). Investigations on integrated funnel, fan and diffuser augmented unique wind turbine to enhance the wind speed. *Journal of Applied Fluid Mechanics*, 16(3), 575-589. <https://doi.org/10.47176/jafm.16.03.1498>
- Rehman, S., Alam, M., Alhems, L. M., Rafique, M. M., et al. (2018). Horizontal axis wind turbine blade design methodologies for efficiency enhancement—a review. *Energies*, 11(3), 506. <https://doi.org/10.3390/en11030506>
- Rhodes, C. J. (2016). The 2015 paris climate change conference: Cop21. *Science Progress*, 99(1), 97–104. <https://doi.org/10.3184/003685016x14528569315192>
- Schepers, J., Boorsma, K., & Munduate, X. (2014). *Final results from mexnext-i: Analysis of detailed aerodynamic measurements on a 4.5 m diameter rotor placed in the large german dutch wind tunnel dnr*. Journal of Physics: Conference Series. IOP Publishing. <https://doi.org/10.1088/1742-6596/555/1/012089>
- Shen, W. Z., Mikkelsen, R., Sørensen, J. N., & Bak, C. (2005). Tip loss corrections for wind turbine computations. *Wind Energy*, 8(4), 457–475. <https://doi.org/10.1002/we.153>
- Snel, H. (2003). Review of aerodynamics for wind turbines. *Wind Energy: An International Journal for Progress and Applications in Wind Power Conversion Technology*, 6(3), 203–211. <https://doi.org/10.1002/we.97>
- Snel, H., Houwink, R., Bosschers, J., et al. (1994). *Sectional prediction of lift coefficients on rotating wind turbine blades in stall*. Netherlands Energy Research Foundation Petten, Netherlands.
- Sørensen, J. N., & Myken, A. (1992). Unsteady actuator disc model for horizontal axis wind turbines. *Journal of Wind Engineering and Industrial Aerodynamics*, 39(1-3), 139–149. [https://doi.org/10.1016/0167-6105\(92\)90540-Q](https://doi.org/10.1016/0167-6105(92)90540-Q)
- Stevens, R. J., Martínez-Tossas, L. A., & Meneveau, C. (2018). Comparison of wind farm large eddy simulations using actuator disk and actuator line models with wind tunnel experiments. *Renewable Energy*, 116, 470 – 478. <https://doi.org/10.1016/j.renene.2017.08.072>
- Sturge, D., Sobotta, D., Howell, R., While, A., & Lou, J. (2015). A hybrid actuator disc – full rotor cfd methodology for modelling the effects of wind turbine wake interactions on performance. *Renewable Energy*, 80, 525– 537. <https://doi.org/10.1016/j.renene.2015.02.053>
- Tian, L., Song, Y., Zhao, N., Shen, W., Zhu, C., & Wang, T. (2020). Effects of turbulence modelling in ad/rans simulations of single wind tidal turbine wakes and double wake interactions. *Energy*, 208, 118440. <https://doi.org/10.1016/j.energy.2020.118440>
- Yakhot, V., & Orszag, S. A. (1986). Renormalization group analysis of turbulence. i. basic theory. *Journal of Scientific Computing*, 1(1), 3–51. <https://doi.org/10.1007/bf01061452>